CHEMISTRY OF MATERIALS

Article

pubs.acs.org/cm

Quantification of Site-Specific Cation Exchange in Metal–Organic Frameworks Using Multi-Wavelength Anomalous X-ray Dispersion

Carl K. Brozek,[†,∥] Anthony F. Cozzolino,[†,∥] Simon J. Teat,[‡] Yu-Sheng Chen,[§] and Mircea Dincă*[,†]

[†]Department of Chemistry, Massachusetts Institute of Technology, 77 Massachusetts Avenue, Cambridge, Massachusetts 02139, United States

[‡]Advanced Light Source, Lawrence Berkeley National Laboratory, Berkeley, California 94720, United States

[§]ChemMatCARS, Advanced Photon Source, Argonne National Laboratory, Chicago, Illinois 60439, United States

Supporting Information

ABSTRACT: We employed multiwavelength anomalous X-ray dispersion to determine the relative cation occupation at two crystallographically distinct metal sites in Fe^{2+}-, Cu^{2+}-, and Zn^{2+}-exchanged versions of the microporous metal–organic framework (MOF) known as MnMnBTT (BTT = 1,3,5-benzenetristetrazolate). By exploiting the dispersive differences between Mn, Fe, Cu, and Zn, the extent and location of cation exchange were determined from single crystal X-ray diffraction data sets collected near the K edges of Mn^{2+} and of the substituting metal, and at a wavelength remote from either edge as a reference. Comparing the anomalous dispersion between these measurements indicated that the extent of Mn^{2+} replacement depends on the identity of the substituting metal. We contrasted two unique methods to analyze this data with a conventional approach and evaluated their limitations with emphasis on the general application of this method to other heterometallic MOFs, where site-specific metal identification is fundamental to tuning catalytic and physical properties.

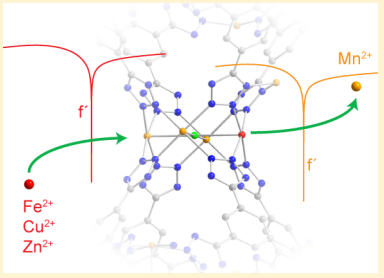

KEYWORDS: *metal–organic frameworks, postsynthetic ion metathesis, anomalous X-ray dispersion*

INTRODUCTION

Post-synthetic ion metathesis (PSIM) has become a prominent method for synthesizing new crystalline materials and is especially powerful for targeting metastable phases that are inaccessible by conventional high temperature synthetic methods.[1−8] Notable recent examples include inorganic nanocrystals and metal–organic frameworks (MOFs), whose nanoscale dimensionality and porosity, respectively, allow rapid replacement of cations in a parent structure at or near room temperature. The parent structures, usually obtained at high temperature under thermodynamic control, template the new phases, which are under kinetic control. By inserting cations into well-defined environments, PSIM enables the rational design of physical properties and chemical reactivity of materials that may otherwise be physically and chemically inactive.[3,5] A clear structure–function understanding is needed to design these materials, though their enhanced structural complexity undermines atomic-level structural characterization. Therefore, developing analytical tools to determine the location and site-occupancy of both the substituting and the parent cations in MOFs formed by PSIM is paramount for establishing this technique as a reliable and rational synthetic method for MOFs.

Herein, we demonstrate that multiwavelength anomalous dispersion (MAD)[9−16] is a powerful method to quantify the extent and location of cation exchange in MOFs with multiple crystallographically independent metal sites, where the cation location is ambiguous. The material investigated here, $Mn_3[(Mn_4Cl)_3(BTT)_8]_2$ (MnMnBTT; BTT = 1,3,5-benzenetristetrazolate),[17] was chosen as a model system because its two crystallographically distinct Mn^{2+} ions can be exchanged for a variety of mono- and divalent metal ions,[18] and because the relatively low energy Mn K edge provides a maximum resolution of 0.94 Å at $\theta = 85°$, the limit of our setup. Our analysis of MnMnBTT outlines key limitations of MAD, providing a guide for its use with other heterometallic MOFs. In the desolvated state of MnMnBTT, one metal site is coordinated equatorially to four nitrogen atoms from four tetrazole rings and to an axially bound chloride anion, which together define an intraframework C_{4v} site. A second metal site is coordinated to two nitrogen atoms defining an extraframework C_s site (Figure 1).[17] Both Mn^{2+} cations exchange with other divalent or monovalent cations, but the location (i.e., C_{4v} versus C_s) and site occupation of the metal substitution could not be demonstrated experimentally and were previously inferred only on the basis of elemental analysis.[18] Using variable wavelength synchrotron radiation, we take advantage of element-specific anomalous X-ray dispersion to locate the extent of Fe^{2+}, Cu^{2+}, and Zn^{2+} incorporation in the intraframework C_{4v} site of MnMnBTT, our benchmark system. We present three methods of analyzing this data to quantify the

Received: March 15, 2013
Revised: June 8, 2013
Published: July 2, 2013

   dx.doi.org/10.1021/cm400858d | *Chem. Mater.* 2013, 25, 2998–3002

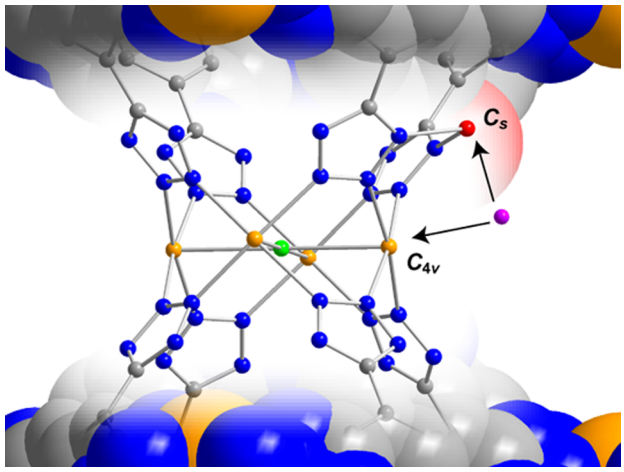

Figure 1. Exchangeable metal sites in M_1M_2BTT. Orange, red, green, blue, and gray spheres represent the C_{4v} metal site, the partially occupied C_s metal site, Cl, N, and C atoms respectively. The pink sphere represents the substituting cation. H atoms have been omitted for clarity.

occupancy of either metal at each site and evaluate their limitations for use with future heterometallic materials.

EXPERIMENTAL SECTION

MATERIALS

N,*N*-dimethylformamide (DMF) (99.8%, Alfa Aesar), $MnCl_2$ (97% Strem), $FeCl_2$ (98% Strem), $CuCl_2$ (≥98% Strem), and $ZnCl_2$ (≥98% Sigma-Aldrich) were used as received. Dry, deaerated methanol (MeOH), and DMF were obtained by degassing with a flow of argon gas for 30 min and by passing the solvent through two silica columns in a Glass Contour Solvent Purification System.

Preparation of MnMnBTT.[17] Colorless MnMnBTT crystals were prepared by sonicating $MnCl_2{\cdot}4H_2O$ (2.8 g, 14 mmol) and $H_3BTT{\cdot}2HCl{\cdot}H_2O{\cdot}MeOH$ (0.62 g, 1.5 mmol) in 140 mL of a 50/50 mixture of MeOH and DMF with 14 drops of concentrated HCl until all solids were completely dissolved. The solution was split equally between 12 scintillation vials and placed in an oven at 70 °C until small cubic crystals began to appear. The vials were transferred to a N_2-filled glovebox and the solutions were decanted. The colorless cubic crystals were rinsed three times with DMF and three times with MeOH in 6 h intervals to prepare them for cation exchange soaks. Three samples were treated, at room temperature (RT, ∼ 20 °C), with MeOH that was replaced 3 times over 3 days to obtain a sample of pristine MnMnBTT that could be activated as a control. The sample was activated by heating under dynamic vacuum for 12 h (4 mtorr, 150 °C) in a prescored ampule which was flame-sealed to preserve the integrity of the activated sample.

Metal Exchange in MnMnBTT.[18] Colorless MnMnBTT crystals were treated with concentrated solutions of $FeCl_2$, $ZnCl_2$, or $CuCl_2$ in MeOH. The samples were soaked for 7 days total, replacing the solution every 2 days. Over the course of 7 days, the $FeCl_2$-soaked MnMnBTT (FeMnBTT) became light yellow, the $ZnCl_2$ soaked MnMnBTT (denoted ZnMnBTT) remained colorless, and the $CuCl_2$ soaked MnMnBTT (denoted CuMnBTT) became dark green. The exchanged samples were treated, at RT (∼ 20 °C), with MeOH that was replaced 3 times over 3 days to remove any excess metal salts prior to activation. The samples were activated by heating under dynamic vacuum for 12 h (4 mtorr, 150 °C) in a prescored ampule which was flame-sealed to preserve the integrity of the activated sample.

Elemental Analysis. Manganese, iron, nickel, copper, and zinc analyses were conducted at the MIT Center for Materials Science and Engineering Shared Experimental Facility (CMSE-SEF) using a HORIBA Jobin ACTIVA inductively coupled plasma atomic emission spectrometer (ICP-AES). Solutions of standard concentrations were prepared from solutions purchased from ULTRA Scientific, designated suitable for ICP analysis.

X-ray Absorption Spectroscopy (XAS). To determine the true K-edge values for the metals in each sample, X-ray absorption spectra were collected over a window spanning 100 eV above and below the reported values for the zerovalent metals. All spectra were collected at beamline 11.3.1 at the Advanced Light Source of Lawrence Berkeley National Laboratory using a Si(111) monochromator and an International Radiation Detectors Inc. AXUV100 photodiode detector. All data collections were taken in transmission mode at 1 eV intervals with powder samples that were appended to the detector with Kapton tape. The minimum in the real component of the scattering factor, f', was taken as the midpoint of the absorption edge. Data was collected 10 eV below this edge to minimize the changes in f'' and the effects of beam instability at the edge where the slope of f' is steepest.

Multiwavelength Anomalous Dispersion. A single crystal suitable for X-ray diffraction was chosen for each sample and mounted on a kapton loop. Data sets were collected at 100(2) K at ChemMatCARS and at beamline 11.3.1 of the Advanced Light Source of Lawrence Berkeley National Laboratory using a double Si(111) monochromator with a Bruker AXS APEXII CCD and Bruker D8 diffractometer. The X-ray intensity was attenuated by physically blocking the beam path with filters of varying absorption strength until the CCD detector remained unsaturated. Optimal attenuation filters were chosen to maximize the intensity for each shell that was collected. Data sets were collected at wavelengths corresponding to 10 eV lower than the maximum f' values of the transition metals present in each sample as determined by the XAS experiments described above (see Figure 2). An additional data set was collected for each sample at 0.775 Å for overall structure determination.

Data Reduction. A preliminary unit cell was determined for each data set by harvesting spots with $I > 10\sigma$ for a subset of the collected frames. The data was integrated by averaging the peak shape from each detector region and using a mask software[19] to remove the shadow of the beamstop. The unit cell was periodically updated using triclinic parameters. Integration was repeated after reading in the updated unit cell from the unmerged .p4p file. The data was scaled using SADABS[20] following the default settings with the exception of choosing the *m3m* Laue group, increasing the restraint estimated standard deviations for equal consecutive scale factors to 0.02, and applying an angle of incidence correction. The crystals were not indexed, and therefore a numerical absorption correction could not be applied. In the final reflection file the Bijvoet pairs were kept separate. The structure solution was determined by either direct methods or by performing a Patterson heavy atom search in the case of a failure by direct methods to obtain a reasonable solution. The structure of each

dx.doi.org/10.1021/cm400858d | *Chem. Mater.* 2013, 25, 2998−3002

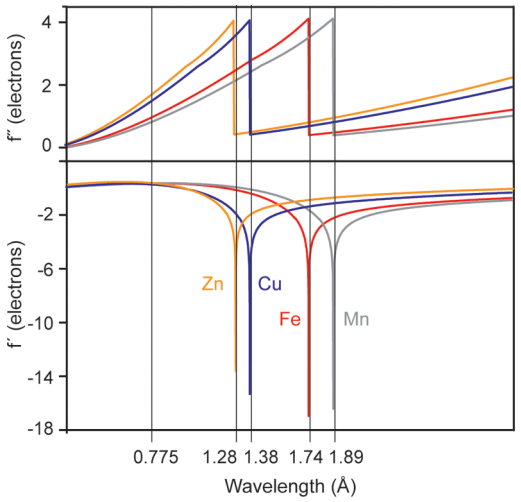

Figure 2. Curves f' and f'' derived from the Kramers–Kronig relation[23] shown in color, with the incident wavelengths delineated by vertical lines.

framework was fully refined against the 0.775 Å data set using SHELXL.[21] Residual density within the pores, aside from a partially occupied O atom of a bound methanol molecule, was not sufficiently localized to allow modeling. This residual density was not refined and does not represent a sizable contribution because the material was activated prior to collection.

Data Analysis. Three independent methods were used to quantify the composition at the C_{4v} metal site. The real and imaginary components (f' and f'') of the anomalous dispersion modify the atomic scattering factor $f(hkl, \lambda_M)$ according to eq 1. These factors cause an apparent decrease or increase in the electron density of an element if the incident wavelength corresponds to its absorption edge. We present two unique data analysis methods, which correlate site occupancy to differences in electron density. The third approach refines against the data sets taken at the three wavelengths simultaneously while refining the occupancy of multiple metals at the same sites.[10]

$$f(000, \lambda_M) = f(000)_M + f'(\lambda_M)_M + if''(\lambda_M)_M \quad (1)$$

Refined Occupancy Difference (ROD) Method. The structure was solved and refined at a wavelength distant from a relevant absorption edge, while correcting for the anomalous dispersion of C, N, O, and Cl. Once this model was refined with the C_{4v} metal site fully occupied with Mn, this same model was refined against all the wavelengths with the appropriate dispersion corrections for C, N, O, and Cl while allowing the occupancy of the C_{4v} site to refine freely. The final occupancy was multiplied by the expected number of electrons for the element used during the refinement, giving the apparent electron density $\rho_{app}(M)$ at incident wavelengths near the K edges of M = Mn, Fe, Cu, or Zn.

Integrated Density Difference (IDD) Method. The structure was solved and fully refined against the remote wavelength data collected at 0.775 Å with the appropriate anomalous dispersion corrections for C, N, O, and Cl. This model was refined against the data sets collected at the K edges of Mn and the other metal to produce a structure factor file (SHELX type 6). A Fast Fourier Transform was applied to this file using the WinGX program suite with a grid spacing of 0.05 Å[22] to give the experimental relative electron densities. These values of arbitrary magnitude were scaled to the electron density of the nitrogen atoms because the anomalous dispersion coefficients of N are relatively invariant to the wavelengths used in this series of experiments. This scaling procedure provided apparent electron densities $\rho_{app}(\lambda_M)$.

For both ROD and IDD methods, the ratio of the two metals at the C_{4v} site in each material could be determined from eqs 1–4, where α is the fraction of Mn or M at the site of interest, $|f(000, \lambda_{Mn})_M|$ is the magnitude of the atomic scattering factor at $|hkl| = |000|$ for metal M near the K edge of Mn, $f'(\lambda_{Mn})_M$ is the real component of the anomalous dispersion coefficient for metal M near the wavelength corresponding to the Mn absorption edge (and vice versa), $f''(\lambda_{Mn})_M$ is the imaginary component of the anomalous dispersion coefficient for metal M at a wavelength near the Mn absorption edge (and vice versa), and k is a scaling factor to recover the electron density at each edge due to the combination of metals in the site of interest.

Fractional occupancies of site

$$\alpha_{Mn} + \alpha_M = 1 \quad (2)$$

Anomalous dispersion at Mn edge

$$\alpha_{Mn}|f(000, \lambda_{Mn})_{Mn}| + \alpha_M|f(000, \lambda_{Mn})_M| = k\rho_{app}(\lambda_{Mn}) \quad (3)$$

Anomalous dispersion at M edge

$$\alpha_{Mn}|f(000, \lambda_M)_{Mn}| + \alpha_M|f(000, \lambda_M)_M| = k\rho_{app}(\lambda_M) \quad (4)$$

Simultaneous Multiwavelength Occupancy Refinement (SMOR) Method. Here, we refined the model against all the data sets simultaneously with both possible metals at the C_{4v} site and allowed their occupancies to refine under the constraint that the total site occupation does not exceed unity. Anomalous dispersion coefficients were estimated from the theoretical dispersion curves given by the Kramers–Kronig relation[23] by selecting values that were 10 eV lower in energy from the f' minimum. This directly gave a metal ratio for the occupation of the C_{4v} site. The freely available software JANA was used for this refinement.[24]

RESULTS AND DISCUSSION

Crystals of MnMnBTT were prepared according to a literature procedure[17] and soaked in methanol solutions of anhydrous $FeCl_2$, $CuCl_2$, or $ZnCl_2$ for 7 days to afford FeMnBTT, CuMnBTT, or ZnMnBTT. To eliminate the possibility of extraneous metals residing within the pores as was previously observed,[18] we performed three successive three-day soaks in clean methanol, then desolvated the samples at 150 °C until a pressure of less than 4 mtorr could be maintained for 10 min under static vacuum. Each sample was protected with degassed Paratone-N oil and mounted under a 100 K N_2 stream. For each sample a full data set was collected at 0.775 Å from which the structure was solved and refined.

Single crystal X-ray diffraction data sets were collected for a MnMnBTT single crystal at wavelengths 10 eV lower than the K edges of Fe, Mn, Cu, and Zn, as determined by X-ray absorption spectroscopy of the substituted samples (1.898 Å, 1.744 Å, 1.381 Å, 1.284 Å for Mn, Fe, Cu, and Zn, respectively). These incident wavelengths are depicted in Figure 2 alongside the theoretical f' and f'' curves. A reference data set was also collected at 0.775 Å, remote from the edges of these elements, where the anomalous scattering factors are indistinguishable.[25] For the exchanged materials, FeMnBTT, CuMnBTT, and

dx.doi.org/10.1021/cm400858d | Chem. Mater. 2013, 25, 2998–3002

ZnMnBTT, data sets were collected at the Mn K edge, the substituting metal K edge, and at 0.775 Å.

To analyze the substituted materials, we established the behavior of the unsubstituted MnMnBTT with MAD since its metal occupancies were known. This control experiment allowed us to observe how $f(000, \lambda_M)$ deviates from the theoretical values at each wavelength in the absence of substituted cations, which is necessary for later contextualizing the apparent changes in $f(000, \lambda_M)$ of the substituted materials. To evaluate the IDD and ROD methods, we used the final apparent electron density, $\rho_{app}(\lambda_M)$, at each K edge wavelength to calculate the ratio of Mn to the corresponding transition metal in the C_{4v} site (see eqs 1-4). Using the SMOR method, the ratio of metals was available directly.

The relative metal occupancies derived from all three methods are provided in Table 1 for MnMnBTT and reveal

Table 1. Unit Cell Parameters and C_{4v} Metal Site Occupancy Data for MnMnBTT-7d Collected at Fe, Cu, and Zn Edges Shown as M%

MnMnBTT	λ = Fe	λ = Cu	λ = Zn
unit cells (Å)	18.9153(5)	18.9153(5)	18.9153(5)
ICP-AES	0	0	0
IDD	10.1	2.3	0.3
ROD	13.2	2.1	0.3
SMOR	−14.9(4)	−11.7(3)	−9.6(3)

that the methods each have intrinsic error as they all deviate from a substituting metal occupancy of 0%. In the IDD and ROD methods, the Fe, Cu, or Zn occupancies, which are necessarily zero under the synthetic conditions, give positive nonzero values. The largest error occurs for the data evaluated at the Fe edge, which is likely due to the proximity of the Fe and Mn edges (see Figure 2). Both Cu and Zn have values that are closer to the expected 0%. The SMOR method tends to underestimate the occupancies such that Mn occupancies are greater than unity, which cannot be accounted for by the standard uncertainty in the refined value. Taken together, this control experiment provides a baseline uncertainty in ascribing deviations in $f(000, \lambda_M)$ to the occupancy of substituting cations with FeMnBTT, CuMnBTT, and ZnMnBTT.

As shown in Table 2, cation exchange for 7 days with MnMnBTT produced materials with significantly changed unit

Table 2. Unit Cell Parameters and C_{4v} Metal Site Occupancy Data for MMnBTT-7d (M = Fe, Cu, and Zn) Shown as M%[a]

MMnBTT	M = Fe	M = Cu	M = Zn
unit cells (Å)	19.0218(5)	18.4852(5)	18.8285(4)
ICP-AES	3.2	88.8	74.8
IDD	19.5 [9.4]	102.4 [100.1]	100.7 [100.4]
ROD	7.2 [-6.0]	106.9 [104.8]	100.8 [100.5]
SMOR	−7.8(5) [7.2]	88.3(3) [100.0]	66.2(4) [75.8]

[a]M% corrected for baseline from MnMnBTT.

cell parameters, with the exception of FeMnBTT, whose unit cell edge was 19.0218(5) Å. This value is more consistent with that of the parent MnMnBTT structure, 19.009(1) Å,[17] than with the all iron analogue, FeFeBTT, which has a cell parameter of 18.824(1) Å.[26] The small difference between the unit cell dimensions of FeMnBTT and MnMnBTT suggests that Fe^{2+} exchanged minimally into the intraframework C_{4v} site after soaking for 7 days because the unit cell dimensions of MMnBTT are sensitive to changes in the metal−nitrogen bonds of the C_{4v} site, not changes in the C_s site. In contrast, CuMnBTT and ZnMnBTT prepared by week-long soaks showed unit cell parameters of 18.4852(5) Å and 18.8285(4) Å, respectively. The former value is closer to that of all-copper CuCuBTT, 18.595(7) Å,[27] which indicates the significant incorporation of Cu^{2+} at the C_{4v} sites, as had been previously proposed on the basis of elemental analysis.[28]

MAD analysis of FeMnBTT, also summarized in Table 2, corroborates the ICP-AES and unit cell analysis above that Fe^{2+} exchanges marginally in to the C_{4v} site. The metal content evaluated from each method reveals Fe occupations at the C_{4v} site ranging from −7.8% to 19.5%. The results of each method are compared to the ICP-AES data, which gives an Fe content of 3.2%, assuming that Fe^{2+} exchanges the charge-balancing C_s completely. These values can be improved by normalizing them to the occupancies derived from the control experiment (as shown in Table 1). This recalculation gives values of 9.4%, −6.0%, and 7.2% for the IDD, ROD, and SMOR methods, respectively. Despite the large variation between methods, they provide a consistent depiction of limited Fe^{2+} exchange at the C_{4v} metal site.

MAD analyses of the Cu^{2+} and Zn^{2+} exchanges indicate that they incorporate to a much greater extent into the C_{4v} site than Fe^{2+}, which agrees with the previously proposed formulas.[18] Assuming that both metals exchange the C_s site completely, the ICP-AES values for the C_{4v} sites, as shown in Table 2, suggest Cu^{2+} occupies 88.8% of those sites, while Zn^{2+} occupies 74.8%. On the other hand, MAD analysis suggests that the occupancy of Cu^{2+} ranges from 88.3−106.9%. After normalizing to the occupancies derived from the MnMnBTT control, the values adjust to 100.1, 104.8, and 100.0% for the IDD, ROD, and SMOR methods, respectively. The Zn^{2+} occupancy ranges from 66.2−100.8% between the three methods. The corrected values become 100.4%, 100.5%, and 75.8% for the IDD, ROD, and SMOR methods, respectively, which are more consistent with the ICP-AES data assuming a fully Zn^{2+} occupied C_s site.

In conclusion, multiwavelength anomalous dispersion is the only site-specific method for discerning site occupancy of metals with similar atomic numbers and electron density in MOFs. We presented two novel methods for analyzing the data, in addition to a previously reported method, and demonstrated their reliability so that meaningful conclusions could be drawn for more general examples. All three methods suffered from an inherent error as established by a control experiment, which could be minimized by performing the measurements on-edge to maximize f', as well as ∼10 eV above and below this value to maximize and minimize the f'' value. Because X-ray diffraction data collected near the Mn K edge inherently limits the resolution, we expect that the errors obtained for materials with heavier atoms would be minimized. Therefore, the series of materials derived from MnMnBTT define a lower limit of precision for quantitative MAD analysis, and show that the latter provides a practical account of the location and extent of cation exchange, especially when coupled with elemental analysis. In future studies centered on the reactivity and physical properties of heterobi- and multimetallic MOFs made by PSIM, this method will prove valuable in providing definitive correlations between structure and function.

dx.doi.org/10.1021/cm400858d | Chem. Mater. 2013, 25, 2998−3002

■ ASSOCIATED CONTENT

Supporting Information

Crystallographic data in CIF format. This material is available free of charge via the Internet at http://pubs.acs.org.

■ AUTHOR INFORMATION

Corresponding Author

*E-mail: mdinca@mit.edu.

Author Contributions

‖These authors contributed equally.

Notes

The authors declare no competing financial interest.

■ ACKNOWLEDGMENTS

This research was supported by the U.S. Department of Energy, Office of Science, Office of Basic Energy Sciences, under Award DE-SC0006937. C.K.B gratefully acknowledges the NSF Graduate Research Fellowship Program for financial support through Grant 1122374. We are grateful for the use of beamline 15-ID-B,C,D at the Advanced Photon Source and beamline 11.3.1 at the Advanced Light Source. ChemMatCARS Sector 15 is principally supported by the National Science Foundation/Department of Energy under Grant NSF/CHE-0822838. Use of the Advanced Photon Source, an Office of Science User Facility operated for the U.S. Department of Energy (DOE) Office of Science by Argonne National Laboratory, was supported by the U.S. DOE under Contract No. DE-AC02-06CH11357. The Advanced Light Source is supported by the Director, Office of Science, Office of Basic Energy Sciences, of the U.S. Department of Energy under Contract No. DE-AC02-05CH11231.

■ REFERENCES

(1) Rivest, J. B.; Jain, P. K. *Chem. Soc. Rev.* **2013**, *42*, 89−96.

(2) Kim, Y.; Das, S.; Bhattacharya, S.; Hong, S.; Kim, M. G.; Yoon, M.; Natarajan, S.; Kim, K. *Chem.—Eur. J.* **2012**, *18*, 16642−16648.

(3) Brozek, C. K.; Dincă, M. *Chem. Sci.* **2012**, *3*, 2110−2113.

(4) Denysenko, D.; Werner, T.; Grzywa, M.; Puls, A.; Hagen, V.; Eickerling, G.; Jelic, J.; Reuter, K.; Volkmer, D. *Chem. Commun.* **2012**, *48*, 1236−1238.

(5) Zhang, Z.; Zhang, L.; Wojtas, L.; Nugent, P.; Eddaoudi, M.; Zaworotko, M. J. *J. Am. Chem. Soc.* **2012**, *134*, 924−927.

(6) Luther, J. M.; Zheng, H.; Sadtler, B.; Alivisatos, A. P. *J. Am. Chem. Soc.* **2009**, *131*, 16851−16857.

(7) Robinson, R. D.; Sadtler, B.; Demchenko, D. O.; Erdonmez, C. K.; Wang, L.-W.; Alivisatos, A. P. *Science* **2007**, *317*, 355−358.

(8) Son, D. H.; Hughes, S. M.; Yin, Y.; Paul Alivisatos, A. *Science* **2004**, *306*, 1009−1012.

(9) Wu, G.; Zhang, Y.; Ribaud, L.; Coppens, P.; Wilson, C.; Iversen, B. B.; Larsen, F. K. *Inorg. Chem.* **1998**, *37*, 6078−6083.

(10) Helliwell, M.; Helliwell, J. R.; Kaucic, V.; Zabukovec Logar, N.; Teat, S. J.; Warren, J. E.; Dodson, E. J. *Acta Crystallogr., Sect. B: Struct. Sci.* **2010**, *66*, 345−357.

(11) Einsle, O.; Andrade, S. L. A.; Dobbek, H.; Meyer, J.; Rees, D. C. *J. Am. Chem. Soc.* **2007**, *129*, 2210−2211.

(12) Freedman, D. E.; Han, T. H.; Prodi, A.; Müller, P.; Huang, Q.-Z.; Chen, Y.-S.; Webb, S. M.; Lee, Y. S.; McQueen, T. M.; Nocera, D. G. *J. Am. Chem. Soc.* **2010**, *132*, 16185−161890.

(13) Wilkinson, A. P.; Cheetham, A. K.; Tang, S. C.; Reppart, W. J. *J. Chem. Soc., Chem. Commun.* **1992**, 1485−1487.

(14) Hodeau, J.-L.; Favre-Nicolin, V.; Bos, S.; Renevier, H.; Lorenzo, E.; Berar, J.-F. *Chem. Rev.* **2001**, *101*, 1843−1868.

(15) Helliwell, M.; Helliwell, J. R.; Kaucic, V.; Zabukovec Logar, N.; Barba, L.; Busetto, E.; Lausi, A. *Acta Crystallogr., Sect. B: Struct. Sci.* **1999**, *55*, 327−332.

(16) Helliwell, M. *J. Synchrotron Rad.* **2000**, *7*, 139−147.

(17) Dincă, M.; Dailly, A.; Liu, Y.; Brown, C. M.; Neumann, D. A.; Long, J. R. *J. Am. Chem. Soc.* **2006**, *128*, 16876−16883.

(18) Dincă, M.; Long, J. R. *J. Am. Chem. Soc.* **2007**, *129*, 11172−11176.

(19) Contact Yu-Sheng Chen, ChemMatCARS, The University of Chicago; yschen@cars.uchicago.edu.

(20) Sheldrick, G. M. *SADABS: Program for Empirical Absorption Correction of Area Detectors*; Bruker AXS: Madison, WI, 1996.

(21) Sheldrick, G. M. *SHELX97 [Includes SHELXS97, SHELXL97, CIFTAB]: Programs for Crystal Structure Analysis*, release 97-2; Bruker AXS: Madison, WI, 1998.

(22) Farrugia, L. J. *J. Appl. Crystallogr.* **1999**, *32*, 837−838.

(23) Kissel, L.; Pratt, R. H. *Acta Crystallogr., Sect. A* **1990**, *46*, 170−175.

(24) Petricek, V.; Dusek, M.; Palatinus, L. *JANA2006*; Institute of Physics: Prague, Czech Republic, 2006.

(25) Chantler, C. T.; Olsen, K.; Dragoset, R. A.; Chang, J.; Kishore, A. R.; Kotochigova, S. A.; Zucker, D. S. X-Ray Form Factor, Attenutaion, and Scattering Tables; http://www.nist.gov/pml/data/ffast/index.cfm (accessed Mar 3, 2013).

(26) Sumida, K.; Horike, S.; Kaye, S. S.; Herm, Z. R.; Queen, W. L.; Brown, C. M.; Grandjean, F.; Long, G. J.; Dailly, A.; Long, J. R. *Chem. Sci.* **2010**, *1*, 184−191.

(27) Dincă, M.; Han, W. S.; Liu, Y.; Dailly, A.; Brown, C. M.; Long, J. R. *Angew. Chem., Int. Ed.* **2007**, *46*, 1419−1422.

(28) An independently synthesized all zinc analogue, ZnZnBTT, has not yet been reported, and the unit cell of such a compound is therefore unknown.